A&A 560, A36 (2013)
DOI: 10.1051/0004-6361/201321815

Astronomy & Astrophysics

Viscous dissipation in 3D spine reconnection solutions

I. J. D. Craig and N. Lopez

Department of Mathematics, University of Waikato, PB 3105 Hamilton, New Zealand
e-mail: nl89@students.waikato.ac.nz

Received 2 May 2013 / Accepted 23 September 2013

ABSTRACT

Aims. We consider the influence of viscous dissipation on "spine" reconnection solutions in coronal plasmas. It is known from 2D and 3D "fan" reconnection studies that viscous losses can be important. We extend these arguments to 3D "spine" reconnection solutions.
Methods. Steady 3D spine reconnection models were constructed by time relaxation of the governing visco-resistive MHD equations. Scaling laws were derived that compare the relative importance of viscous and resistive damping.
Results. It is shown that viscous dissipation in spine reconnection models can dominate resistive damping by many orders of magnitude. A similar conclusion, but with less severe implications, applies to current sheet "fan" solutions. These findings are not sensitive to whether classical or Braginskii viscosity is employed.

Key words. Sun: flares – magnetic reconnection – magnetohydrodynamics (MHD)

1. Introduction

Energy losses in magnetic coronal plasmas are often rapid and violent – witness the solar flare. Flare signatures include hot, X-ray emitting plasmas, strong mass motions, and the acceleration of non-thermal particles (Priest & Forbes 2000). Although magnetic reconnection is thought to be the primary energy release mechanism, it is now recognised that reconnection can take a variety of forms, depending on the details of the field geometry. It also seems likely that purely resistive reconnection mechanisms may have to be augmented by other physical processes – for instance, collisionless, turbulent or viscous effects – if the stringent energetic demands of flare plasmas are to be met (Cassak et al. 2006; Kowal et al. 2009; Craig & Litvinenko 2012).

The purpose of the present paper is to examine the role of viscous dissipation on 3D "spine" magnetic reconnection solutions. We recall that magnetic merging at an isolated 3D magnetic null can take "fan" and "spine" forms (Lau & Finn 1990), depending on whether current sheets or quasi-cylindrical current tubes are involved. These forms derive from the eigenstructure of the null (Priest & Titov 1996) and can be represented by exact magnetohydrodynamic (MHD) solutions, at least in the case of inviscid, incompressible plasmas (Craig & Fabling 1996). An important aspect of these solutions is their ability to provide self-consistent electric and magnetic fields for use in particle acceleration calculations (Heerikhuisen et al. 2002; Litvinenko 2006; Stanier et al. 2012). Since strong acceleration occurs primarily in the vicinity of the magnetic null it is vital to understand the relative roles of spine and fan reconnection.

To date most attention has been focused on the properties of fan reconnection models (Wyper & Pontin 2013), possibly because tubular spine currents seem relatively poorly suited to strong Ohmic dissipation (Craig et al. 1997). Our present concern is that the impact of viscous damping in spine reconnection models has been largely ignored. This neglect contrasts markedly with fan solutions which seem relatively well developed in terms of their energetic and particle acceleration capabilities.

The present paper aims to show that viscous dissipation in spine reconnection solutions is likely to be appreciable, possibly accounting for a significant fraction of the flare energy release. As background we note that recent studies have shown that viscous losses associated with current sheet reconnection are likely to dominate resistive dissipation (Litvinenko 2005; Armstrong et al. 2012). This is true for a range of merging geometries and is largely independent of whether classical viscosity or the more accurate Braginskii (1965) form is employed. Specifically if $\mathcal{W}_\eta$ and $\mathcal{W}_\nu$ represent the global resistive and viscous losses respectively, then their ratio scales as

$$\frac{\mathcal{W}_\nu}{\mathcal{W}_\eta} \sim \frac{\nu}{\eta^{1/2}}. \tag{1}$$

For plausible values of the dimensionless dissipation coefficients ($\nu \gg \eta$ in coronal plasmas) we find that $\mathcal{W}_\nu \gg \mathcal{W}_\eta$. In the present study we investigate how this relation is modified in the case of visco-resistive spine reconnection.

In Sect. 2 we introduce the dimensionless MHD equations and the analytic spine reduction that forms the basis of our study. Our main results are established in Sect. 3, where we begin by discussing analytically the ideal spine system and the steady inviscid axisymmetric spine solution. We then go on to develop, by time relaxation, steady numerical solutions of the full visco-resistive system. Our conclusions are presented in Sect. 4.

2. Spine reconnection equations

2.1. The incompressible MHD equations

The equations to be resolved are the non-dimensional momentum and induction equations for the velocity and magnetic fields $\boldsymbol{v}(\boldsymbol{r}, t)$, $\boldsymbol{B}(\boldsymbol{r}, t)$, namely

$$\partial_t \boldsymbol{v} + \boldsymbol{v} \cdot \nabla \boldsymbol{v} = \boldsymbol{J} \times \boldsymbol{B} - \nabla P + \nabla \cdot \mathcal{S}, \tag{2}$$

$$\partial_t \boldsymbol{B} = \nabla \times (\boldsymbol{v} \times \boldsymbol{B}) - \eta \nabla \times \boldsymbol{J}, \tag{3}$$

together with the constraints

$$\nabla \cdot \boldsymbol{B} = \nabla \cdot \boldsymbol{v} = 0. \tag{4}$$

Here P is the plasma pressure, $\nabla \cdot \mathcal{S}$ is the viscous force and $\boldsymbol{J} = \nabla \times \boldsymbol{B}$ the current density. The equations are scaled with respect to typical solar coronal values for field strength $B_c = 10^2$G, size scale $l_c = 10^{9.5}$cm and number density $n_c = 10^9$cm^{-3}. Times are measured in units of l_c/v_A where $v_A \simeq 10^9$cm s^{-1} is the Alfvén speed.

Energy losses occur through resistive and viscous dissipation. The collisional resistive coefficient is very small – it is an inverse Lundquist number of order 10^{-14} – but since topological change requires finite resistivity it cannot be ignored. Various authors have suggested however that the resistivity may be non-collisionally enhanced by factors approaching one million (see for example Somov & Titov 1983). In the present study we generally assume $\nu \gg \eta$ when comparing viscous and resistive losses. This assumption is easily met even for strongly enhanced "anomalous" resistivities.

Viscous losses depend on the form of the tensor $\mathcal{S}$. This is traditionally represented by the isotropic form

$$\mathcal{S}_{ij} = \nu(\partial_j v_i + \partial_i v_j), \tag{5}$$

where the dimensionless viscous coefficient varies from $10^{-4} \leq \nu \leq 10^{-2}$ for coronal temperatures spanning $2{-}10 \times 10^6$ K (Spitzer 1962). The assumption of isotropy breaks down, however, in magnetic coronal plasmas where the proton mean free path greatly exceeds the proton gyro radius. The anisotropic Braginskii (1965) form, namely

$$\mathcal{S}_{ij} = \nu_0 \left(3\frac{B_i B_j}{B^2} - \delta_{ij}\right)\left(\frac{B_m B_k}{B^2}\,\partial_k v_m\right), \tag{6}$$

(summation over repeated suffixes is assumed) allows for the fact that the cross field viscosity is strongly suppressed (Hollweg 1986; Hosking & Maranoff 1973).

In the present study we are interested in comparing the global viscous and resistive losses under a variety of conditions:

$$\mathcal{W}_\nu = \int \mathcal{S}{:}\nabla \boldsymbol{v}\, \mathrm{d}V, \qquad \mathcal{W}_\eta = \eta \int J^2\, \mathrm{d}V, \tag{7}$$

where $\mathcal{S}{:}\nabla \boldsymbol{v} \equiv \mathcal{S}_{ij}\partial_j v_i$. We generally employ the simpler isotropic viscosity for numerical purposes but revisit the Braginskii form in certain special cases. We follow the usual practices of neglecting the relatively weak anisotropies that occur in the electrical resistivity.

The global losses are conveniently measured in units of $v_A\, l_c{}^2 B_c{}^2/(4\pi) \simeq 8 \times 10^{30}$ erg s^{-1}. In these units, an output of 10^{-3} is required to account for a moderate flare requiring around 10^{28} erg s^{-1}.

2.2. Time dependent spine equations

For an inviscid plasma analytic reconnection solutions can be constructed by superposing localised disturbance fields onto a global background field $\boldsymbol{P}(\boldsymbol{r})$. In the case of spine reconnection we consider the forms

$$\boldsymbol{v} = \alpha \boldsymbol{P} + W(x, y, t)\hat{\boldsymbol{z}}, \quad \boldsymbol{B} = \beta \boldsymbol{P} + Z(x, y, t)\hat{\boldsymbol{z}}, \tag{8}$$

where $\alpha > 0$ and β are constants of order unity. The simplest choice for $\boldsymbol{P}$ is the 3D X-point

$$\boldsymbol{P}(\boldsymbol{r}) = -\kappa x\hat{\boldsymbol{x}} - (1-\kappa)y\hat{\boldsymbol{y}} + z\hat{\boldsymbol{z}}, \tag{9}$$

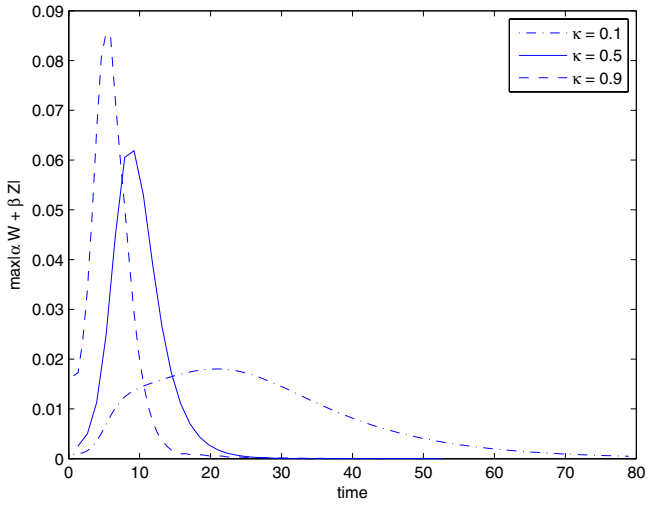

Fig. 1. Relaxation to the steady state $W = -\frac{\beta}{\alpha}Z$ for $\nu = 0$, with $\kappa = 0.1$, 0.5 and 0.9. Parameters of the simulation are $\eta = 0.001$, $\alpha = 1$, $\beta = -0.5$.

where κ defines the isotropy of the null ($0 \leq \kappa \leq 1$). For example with $\kappa = 1$ we obtain a 2D model in which inflow along the x-axis can support a current sheet $Z = Z(x, t)$ aligned to the plane of the exhaust (see Sonnerup & Priest 1975). More generally, the background field is 3D with inflow along the fan ($z = 0$) compensated by exhaust along the spine (the z-axis). This form for $\boldsymbol{P}$ can also be regarded as the leading term in the expansion of a global non-linear field about the null-point.

Substituting forms (8) and (9) into the momentum and induction equations and assuming isotropic viscosity yields

$$W_t = [\mathcal{D}_\kappa - 1](\alpha W + \beta Z) + \nu\nabla^2 W \tag{10}$$

$$Z_t = [1 + \mathcal{D}_\kappa](\beta W + \alpha Z) + \eta\nabla^2 Z \tag{11}$$

where $\mathcal{D}_\kappa$ is the operator

$$\mathcal{D}_\kappa = \kappa x\partial_x + (1-\kappa)y\partial_y. \tag{12}$$

These equations are analysed in detail in the following sections. For the moment it is instructive to consider some key properties of the inviscid system.

2.3. Time-relaxed inviscid solutions

In the case $\nu = 0$ a steady solution with $W = -\beta Z/\alpha$ is easily obtained. The form of Z is then constrained by (11) and a description in terms of special functions is possible in special cases (see the axisymmetric solution of Sect. 3.2). More generally, we can determine inviscid solutions computationally – and assess the dynamic accessibility of the solution – by considering the time relaxation of the system (Tassi et al. 2005).

In Fig. 1 we show the recovery of the steady inviscid solution, from prescribed initial conditions, for three values of κ. Equations (10) and (11) were evolved dynamically, using finite difference replacements, until the system achieved steady state. The plots measure the modulus of $(\alpha W + \beta Z)$ at selected times and demonstrate convergence (to zero) at large t. The simulation assumes the boundary values

$$Z(\pm 1, y, 0) = \pm\frac{g_0}{\sqrt{1+y^2}}, \quad Z(x, \pm 1, 0) = \frac{g_0}{\sqrt{2}}\,x, \tag{13}$$

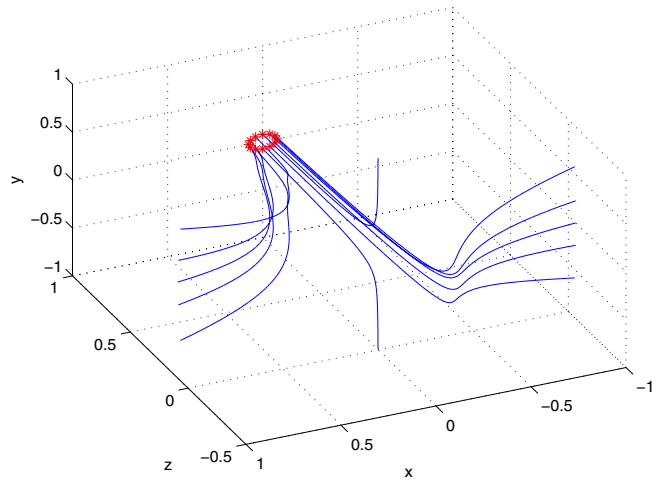

Fig. 2. Magnetic field lines at steady state for $\kappa = 0.6$, with $\eta = 0.003$, $\nu = 0$, $\alpha = 1$, $\beta = -0.5$, $g_0 = 0.015$.

with $Z(x, y, 0) = 0$ elsewhere, and with $W(x, y, 0) = \beta Z(x, y, 0)/\alpha$. These conditions were chosen to be consistent with the reconnective $m = 1$ mode described in Sect. 3.2 and correspond to continuous driving of the disturbance fields. The parameter g_0 controls the strength of the driving and, for the purposes of obtaining resistive scalings, g_0 is typically adjusted to keep the magnitude of the magnetic disturbance field $|Z| \simeq O(1)$.

The spine structure of the magnetic field lines is shown in Fig. 2 for $\kappa = 0.6$. Although, irrespective of κ, the field lines penetrate the fan $z = 0$ for $x > 0$, the field lines in the outer field (projected onto the fan) are strictly radial only for $\kappa = 1/2$.

This behaviour is reinforced in Fig. 3 which shows the movement away from tube-like current structures for $\kappa \neq 1/2$. For $\kappa > 1/2$ in particular, we see that the spine tubes become elongated, leading to more "sheet-like" current structures. Thus $\kappa = 0.8$ corresponds closely to current sheet reconnection, in which inflow of oppositely directed field along the x-axis is balanced by outflow along the spine. The inflow switches mainly to the y-axis for $\kappa = 0.2$. However, as mentioned in Sect. 3.5 below, this solution has a different character in that the initial conditions (13) no longer guarantee that oppositely directed field lines are driven together by the inflow.

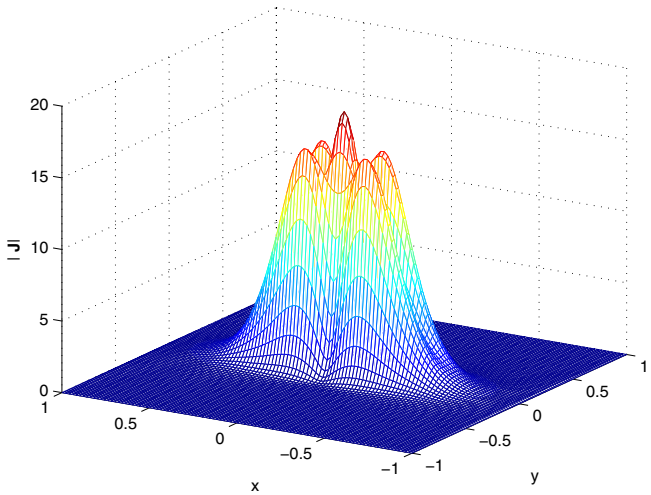

(a) $\kappa = 0.2$

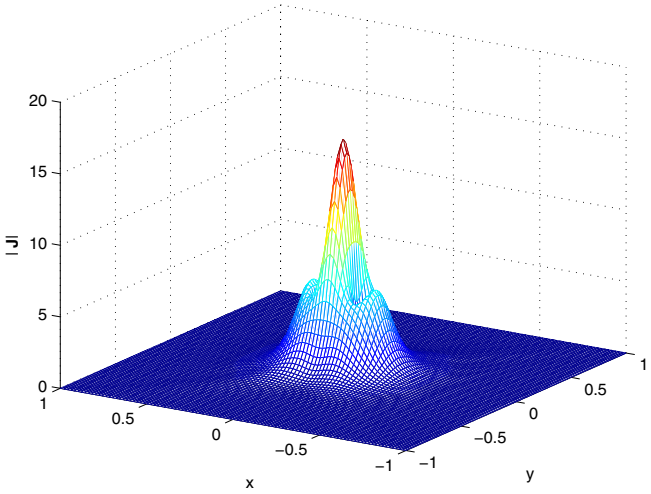

(b) $\kappa = 0.5$

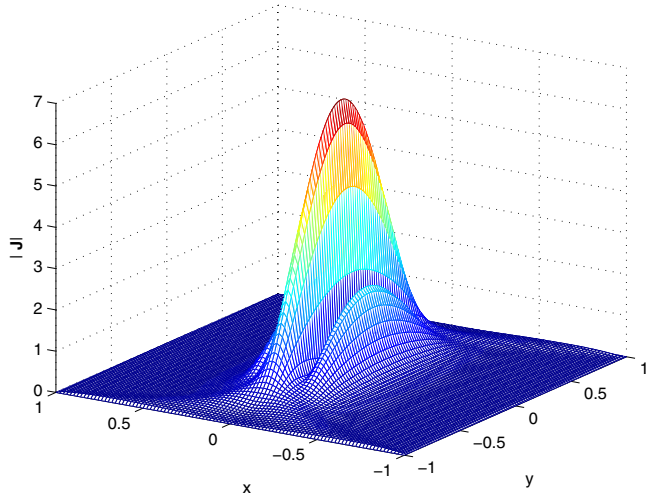

(c) $\kappa = 0.8$

Fig. 3. Current density at steady state for different κ values. In the case $\kappa = 0.8$ the current layer is quasi-one dimensional and closely aligned to the inflow x-axis.

3. Visco-resistive spine reconnection

3.1. The ideal system

To gain analytic insight into the dynamic behaviour of the spine system ((10) and (11)) we first consider the ideal case in which $\eta = \nu = 0$. We anticipate that singularities in the form of unbounded fields can develop along the spine axis which can only be resolved by resistive effects.

We first observe that the operator $\mathcal{D}_\kappa$ defines a directional derivative along the background field. By changing to the characteristic coordinates

$$\xi = \frac{1}{2}\left(\frac{\ln x}{\kappa} + \frac{\ln y}{1-\kappa}\right), \quad \zeta = \frac{1}{2}\left(\frac{\ln x}{\kappa} - \frac{\ln y}{1-\kappa}\right),$$

we obtain the simplification $\mathcal{D}_\kappa \to \partial/\partial\xi$. Introducing the co-moving frame

$$\tau = t, \quad s = \xi - \alpha t, \tag{14}$$

and eliminating W from the system then yields the Klein-Gordon equation

$$Z_{\tau\tau} = \beta^2 Z_{ss} + (\alpha^2 - \beta^2) Z. \tag{15}$$

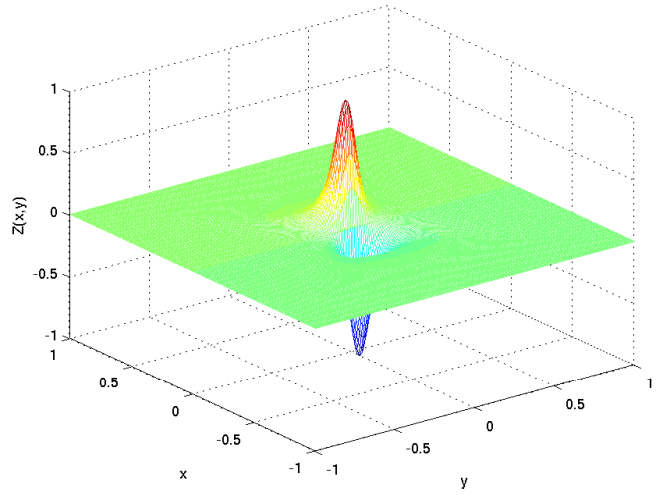

(a) $\beta = -.5$

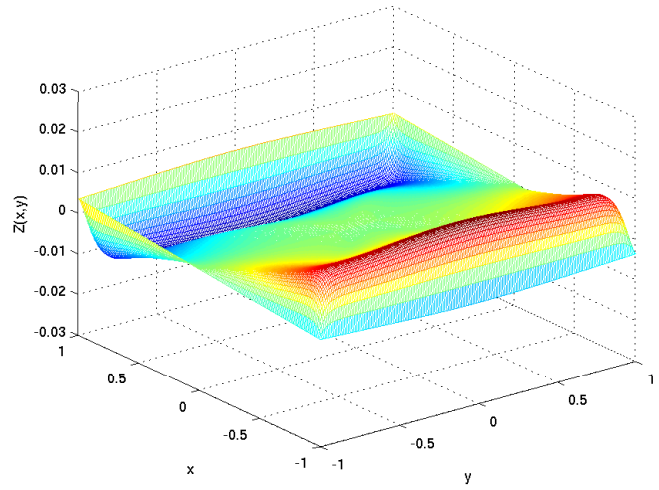

(b) $\beta = -1.1$

Fig. 4. Surface plot of Z field in steady state for $|\beta| < \alpha$ and $|\beta| > \alpha$ respectively, illustrating strong localisation of the field in the former case contrasted with an accumulation in the outer field when $|\beta| = \alpha + 0.1$. Other parameters are $\eta = 0.001$, $\nu = 0.003$, $\alpha = 1$, $\kappa = 0.5$.

Since an identical relation may be found for W, this equation holds for any linear combination of the W and Z disturbances. This equivalence highlights the inherent symmetry in the $\boldsymbol{v}$ and $\boldsymbol{B}$ disturbance fields.

It is interesting that a similar reduction to Klein-Gordon form also occurs for ideal fan reconnection models (Craig & Fabling 1998; Tassi et al. 2005). A key property in all cases is that unbounded exponential growth occurs if $\alpha^2 > \beta^2$. The fastest blow up – as $\exp(\alpha t)$ – occurs when β is negligible. In the isotropic case this corresponds to almost straight field lines, washed in radially, developing as a burgeoning flux rope along the spine. However if $\beta^2 > \alpha^2$ Alfvénic wave modes – the incompressible limit of compressive fast modes – can act to disperse the energy in the disturbance field, thwarting the localisation. In this case flow-driven, compressive flux pile-up reconnection cannot occur.

This change in character of the solution for $\alpha^2 < \beta^2$ is unlikely to be undone by the introduction of small resistive and viscous effects. In Fig. 4, for example, we contrast time relaxations with $|\beta| = \alpha/2$ and $|\beta| = \alpha + 0.1$ keeping all other initial conditions fixed. Well defined solutions are obtained in both cases but the field accumulates in the outer field rather than around the spine for $\beta^2 > \alpha^2$. A similar outer field accumulation occurs for fan solutions when the flow is not sufficiently strong (Craig & Litvinenko 2012).

3.2. The steady axisymmetric solution

Returning to system ((10) and (11)), we now consider the steady resistive solution for axisymmetric inviscid flow. The relation $W = -\beta Z(x, y)/\alpha$ still holds but, rather than seek a Cartesian representation for $Z(x, y)$, it is simplest to adopt a polar decomposition under the assumption of axisymmetry ($\kappa = 1/2$). We then have

$$Z(x, y) \to f(r)\mathrm{e}^{\mathrm{i}m\theta}, \qquad \boldsymbol{P} \to \frac{1}{2}r\hat{\boldsymbol{r}} - z\hat{\boldsymbol{z}} \tag{16}$$

where $r^2 = x^2 + y^2$ and $\tan\theta = y/x$. The differential equation for the radial dependence, namely

$$f + \frac{1}{2}rf' = \bar{\eta}\left(f'' + \frac{f'}{r} - \frac{m^2}{r^2}f\right) \tag{17}$$

has a formal solution, assuming $f \to 0$ as $r \to 0$, given by

$$f(r) = A\left(\frac{r^2}{4\bar{\eta}}\right)^{m/2} M\left(1 + \frac{m}{2},\, 1 + m,\, -\frac{r^2}{4|\bar{\eta}|}\right). \tag{18}$$

Here A is a constant and M is a Kummer function with the properties

$$M(a, b, z) \sim \begin{cases} 1 + \dfrac{a}{b}z \text{ as } \mathrm{z} \to 0 \\ |z|^{-a} \text{ as } \mathrm{z} \to -\infty. \end{cases}$$

In these equations $\bar{\eta} \equiv \eta\alpha/(\alpha^2 - \beta^2)$ and we must take $\alpha > 0$ with $\alpha^2 > \beta^2$ to obtain well behaved spine solutions. All modes have plasma flowing into the fan and exhausted along the spine (as in Fig. 2).

Of prime interest is the reconnection mode associated with the spine solution. The mode $m = 0$ is exceptional in that the null point is displaced along the spine axis resulting in a diffuse current, but all other modes ($m \geq 1$) possess fields localised on the scale ${r_\mathrm{s}}^2 \simeq \eta$ that fall off as $1/r^2$ for large r. The fact that these behave as r^m as $r \to 0$ shows that the current density, namely

$$\boldsymbol{J}(r, \theta) = \left[\mathrm{i}\, m\frac{f(r)}{r}\hat{\boldsymbol{r}} - f'(r)\hat{\boldsymbol{\theta}}\right]\mathrm{e}^{\mathrm{i}m\theta}, \tag{19}$$

can be finite at $r = 0$ only in the case $m = 1$. It follows that $m = 1$ defines the reconnection mode of the spine solution.

3.3. Visco-resistive solutions

With the inclusion of dynamic and viscous effects an exact analytic description is precluded, and solutions must be developed numerically. We follow the time relaxation approach of Sect. 2.3 and adopt the same initial conditions (13). Scaling results are derived by fixing ν while systematically reducing η from 10^{-2} to 3×10^{-5}. This is repeated for $\nu = 0.005$, 0.003 and 0.001. Since an isotropic background field provides the "purest" spine solution, the value $\kappa = 1/2$ will be adopted for the bulk of the numerical simulations in this section.

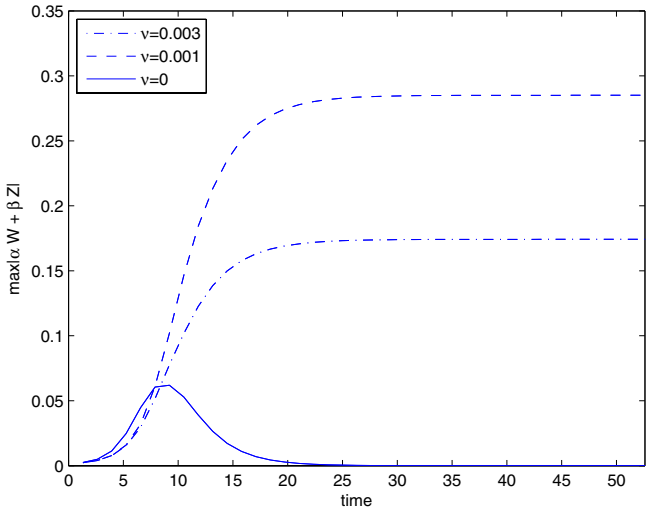

Fig. 5. Effect on the steady state relaxation of adding classical viscosity. The $\nu = 0$ curve is identical to that in Fig. 1, with all other parameters kept fixed ($\eta = 0.001$, $\alpha = 1, \beta = -0.5, \kappa = 0.5$).

Our first observation is that, although the inclusion of viscosity causes the relation $W = -\beta Z/\alpha$ to break down, the qualitative behaviour of the system is largely unaltered. Figure 5, for example, contrasts the relaxation of the inviscid solution with the relaxation for $\nu = 0.001$ and $\nu = 0.003$. Departures from the inviscid relation $W = -\beta Z/\alpha$ increase with ν but this does not compromise the recovery of a well defined, steady solution.

An important question is whether the inclusion of viscosity influences the scaling of the spine current tube. Previous studies (e.g. Park et al. 1984) indicate that a hybrid scale could develop that depends on the product $\eta\nu$. The scaling runs performed below however, suggest that the axisymmetric, inviscid scale $r_s^2 \simeq \eta$ remains robust to the inclusion of viscosity even for $\nu \gg \eta$.

3.4. Ohmic and viscous dissipation rates

To provide a focus for the numerical results we first make an estimate of the global Ohmic losses. We make the provisional assumption that the viscosity has only a minor effect on the scale associated with the localised spine field. In this case $\Delta V \simeq \pi r^2 \simeq \eta$ (Craig et al. 1997) and we find that

$$\mathcal{W}_\eta \simeq \eta J^2 \Delta V \rightarrow \eta {Z_s}^2. \tag{20}$$

For realistic values of the collisional resistivity – and with Z_s of order unity – this rate is far too slow to account for flare-like energy release. Even if the resistivity is enhanced by factors of order 10^6 due to non-collisional effects, the resultant dissipation rate $\mathcal{W}_\eta \simeq 10^{-8}$ remains several orders of magnitude too small.

Viscous dissipation can be calculated directly from (9), which in the case of classical viscosity gives

$$\mathcal{W}_\nu = \nu \int \left(4\alpha^2 \left(\left(\kappa - \frac{1}{2} \right)^2 + \frac{3}{4} \right) + W_x^2 + W_y^2 \right) \mathrm{d}V. \tag{21}$$

Clearly, the first term in the integral represents a constant contribution from the non-uniform background flow required to support the reconnection. For $\kappa \simeq 1/2$ this term yields $\mathcal{W}_\nu = 3\nu\alpha^2 \int \mathrm{d}V$ which gives a power output of around $\mathcal{W}_\nu \simeq 10^{-2}$ in our units (with $\alpha = 1$, $\int \mathrm{d}V = 4$, $\nu = 10^{-3}$). This output translates to global losses of 10^{29} erg s^{-1}, a rate which is clearly sufficient to account for a sizable solar flare. However, the contribution of the reconnection velocity field

$$\nu \int \left(W_x^2 + W_y^2 \right) \mathrm{d}V,$$

should also be taken into account. Since we do not have a sound analytic prediction for this contribution we must rely on extrapolation of our numerical results.

Figure 6 shows that our provisional prediction $\mathcal{W}_\eta \sim \eta$ is well supported by the numerics. For the three values of viscosity modelled (panel a), there is little impact on either the scaling of $\mathcal{W}_\eta$ or its magnitude. Our results show that the viscous dissipation $\mathcal{W}_\nu$ is dominated by the contribution from the background field, which is proportional to ν as per Eq. (21). Specifically, as panel b of Fig. 6 confirms, there is a rapid fall-off of the reconnective component of the velocity field as η becomes

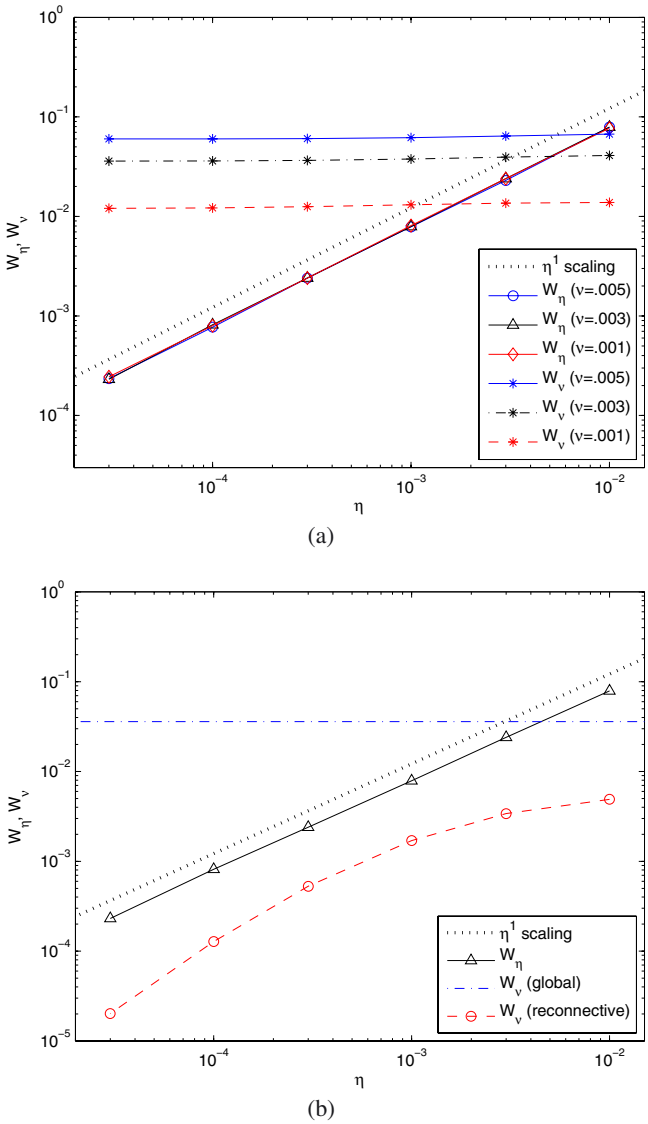

Fig. 6. a) Resistive and viscous dissipation as a function of η for three different values of ν ($\nu = 0.005$, 0.003, 0.001). We note that the Ohmic dissipation rates are effectively unchanged despite the differing values of viscosity. **b)** Resistive and viscous dissipation for $\nu = 0.003$, with the latter separated into contributions from the global background field and the disturbance field. The dotted line indicates η^1 scaling in both panels.

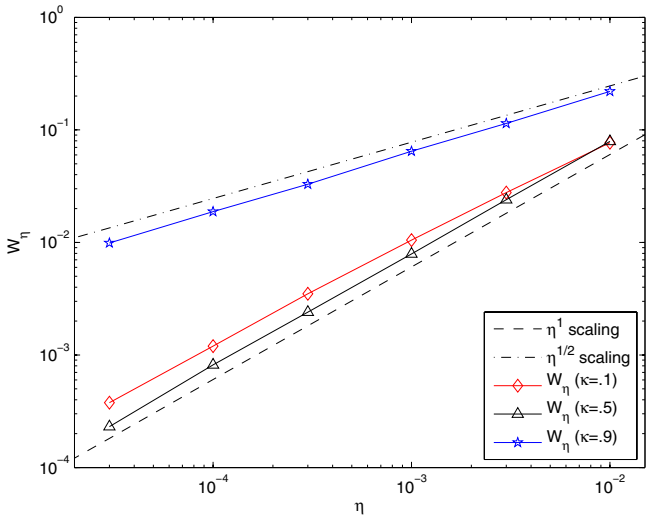

Fig. 7. Scalings for different values of κ. As κ increases from 1/2 towards 1 the scaling changes from η to $\eta^{1/2}$, as given by Eq. (25).

small. This can be understood by observing that, in steady state, the reconnection velocity field (10) should scale as

$$W \simeq \frac{\beta Z}{\alpha + \nu/{r_s}^2}, \tag{22}$$

where r_s is the radial extent of the spine current tube. Taking ${r_s}^2 \simeq \eta$ then implies $W \sim \eta$ provided that $\nu \gg \eta$.

We conclude that, as far as the global energy losses are concerned, the spine current layer provides the main contribution from the magnetic field ($\sim\eta$) whereas the global flow accounts for the bulk of the viscous dissipation ($\sim\nu$). The fact that $\nu \gg \eta$ therefore implies that strong damping of the velocity field can occur even in the presence of very weak reconnection rates.

3.5. Breakdown of axisymmetry

The previous results apply to strictly axisymmetric background fields. When $\kappa \neq 1/2$, the amplitude of background viscous dissipation is altered slightly, but the overall scaling $\mathcal{W}_\nu \sim \nu$ is unaffected (see Eq. (21)). The rates for $\mathcal{W}_\eta$ do, however, vary markedly with κ, as illustrated in Fig. 7. In particular as $\kappa \to 1$ we recover the current sheet scaling $\mathcal{W}_\eta \sim \eta^{1/2}$. The lack of symmetry about $\kappa = 1/2$, perhaps surprising at first sight, can be viewed as an artefact of the initial/boundary conditions since only $\kappa = 1$ corresponds to anti-parallel merging. The limit $\kappa = 0$ is essentially a non-reconnective mode, in which like (as opposed to oppositely directed) fields are driven together. For this reason we concentrate on the range $1/2 \leq \kappa \leq 1$ when developing reconnection scaling laws.

In the regime $1/2 < \kappa < 1$ with $\nu \gg \eta$, it is straightforward to make the estimate

$$\mathcal{W}_\eta \simeq \eta^{1/2\kappa} Z_s^{3-1/2\kappa}, \tag{23}$$

based on the resistive scale $r_s^2 = \eta/\alpha$ and the geometric scaling $\Delta V \simeq \eta^{1/2\kappa}$ (e.g. Craig et al. 1997). This result correctly interpolates between the current sheet ($\kappa = 1$) and the spine reconnection ($\kappa = 1/2$) data.

3.6. Role of the Braginskii viscosity

In general the Braginskii viscosity tensor cannot be incorporated within the analytic spine treatment (8). Since the spine reduction remains valid, however, in the special case $\beta = 0$, we can argue by physical continuity, that this limit should approximate the behaviour of the system for sufficiently small β. A more general treatment probably requires a fully 3D numerical formulation, which we do not pursue here.

In the case $\beta = 0$ the background field is absent and so $\boldsymbol{B} = Z(x, y, t)\hat{\boldsymbol{z}}$. Equation (6) now allows a direct calculation of the viscous dissipation

$$\mathcal{W}_{Brag} = \int 3\nu_0\, \alpha^2\, \mathrm{d}V. \tag{24}$$

Since $\nu_0 \simeq \nu$ we see that Braginskii dissipation is only marginally less effective than the classical losses (21). The implication is that both models of viscosity are capable of providing physically significant damping of the non-uniform velocity fields associated with reconnection.

4. Discussion and conclusions

We have considered 3D visco-resistive spine reconnection for both the classical and Braginskii forms of the fluid viscosity. Steady reconnection solutions were obtained by time relaxation of the governing MHD equations. Although viscosity was found to be ineffective at dissipating energy on the small resistive scale $\sqrt{\eta}$, it did provide effective damping on the global scale of the non-uniform flow that supports the reconnection. While this might eventually be expected to slow the flow enough to stall the reconnection, the associated power output $\mathcal{W}_\nu \simeq 10^{-2}$ is still small compared with the background kinetic energy which is of order unity. We expect therefore that realistic levels of viscous damping will allow the flow to remain strong enough to localise the field while still providing significant levels of viscous dissipation. This conclusion is consistent with recent dynamic reconnection studies in which the current localisation is driven by the Orzag-Tang vortex (Armstrong & Craig 2013).

More specifically, we showed that the ratio of the global viscous losses to the Ohmic losses satisfied

$$\frac{\mathcal{W}_\nu}{\mathcal{W}_\eta} \simeq \frac{\nu}{\eta^{1/2\kappa} Z_s^{1-1/2\kappa}}, \tag{25}$$

where $1/2 \leq \kappa \leq 1$ depends on the isotropy of the merging.

The scaling for $\kappa \simeq 1/2$ in which $\mathcal{W}_\nu/\mathcal{W}_\eta \sim \nu/\eta$ is a new result that derives from the tubular current structures of axisymmetric spine reconnection. This result strengthens previous findings that slow reconnective merging can be associated with flare-like rates of viscous energy dissipation. Yet even for current sheet models where the weaker relation with $\kappa \simeq 1$ holds, global viscous losses should still dominate resistive losses localised to the current layer by several orders of magnitude. This dominance is independent of whether classical or Braginskii viscosity is employed and probably holds good even if the collisional resistivity is enhanced through turbulent effects by factors approaching one million.

It is interesting that the present analysis seems to preclude to the development of a hybrid, visco-resistive scale, typically of the form $(\eta\nu)^{\frac{1}{4}}$ (Park et al. 1984). Models of transient X-point collapse in closed, line-tied, geometries, for instance, are known to develop hybrid scales that significantly weaken the global energy release, in apparent contradiction to the present study (Craig et al. 2005). Such weak rates of energy release, however, emerge only after an initial transient phase in which a significant fraction of the excess X-point energy is viscously dissipated. It seems likely therefore that viscous losses could dominate resistive losses for a wide range of reconnection geometries.

Acknowledgements. We would like to thank Yuri Litvinenko and Craig Armstrong for several helpful comments.

References

Armstrong, C. K., & Craig, I. J. D. 2013, Sol. Phys., 283, 463
Armstrong, C. K., Craig, I. J. D., & Litvinenko, Y. E. 2012, ApJ, 767, 165
Braginskii, S. I. 1965, Rev. Plasma Phys., 1, 205
Cassak, P. A., Drake J. F., & Shay, M. A. 2006, ApJ, 644, L145
Craig, I. J. D., & Fabling, R. B. 1996, ApJ, 462, 969
Craig, I. J. D., & Fabling, R. B. 1998, Phys. Plasmas, 5, 635
Craig, I. J. D., & Litvinenko, Y. E. 2012, ApJ, 747, 16
Craig, I. J. D., Fabling R. B., & Watson, P. G. 1997, ApJ, 485, 383
Craig, I. J. D., Litvinenko, Y. E., & Senanayake, T. 2005, A&A, 433, 1139
Heerikhuisen, J., Litvinkenko, Y. E., & Craig, I. J. D. 2002, ApJ, 566, 512
Hollweg, J. V. 1986, ApJ, 306, 730
Hosking, R. J., & Marinoff, G. M. 1973, Plasma Phys., 15, 327
Kowal, G. Lazarian, A. Vishniac, E. T., & Otmianowska-Mazur, K. 2009, ApJ, 700, 63
Lau, Y. T., & Finn, J. M. 1990, ApJ, 350, 672
Litvinenko, Y. E. 2005, Sol. Phys., 229, 203
Litvinenko, Y. E. 2006, A&A, 452, 1069
Park, W., Monticello, D. A., & White, R. B. 1984, Phys. Fluids, 27, 137
Priest, E. R., & Forbes, T. 2000, Magnetic reconnection: MHD theory and applications (Cambridge Univ. Press)
Priest, E. R., & Titov, V. S. 1996, Roy. Soc. London. Philos. Trans. Ser. A, 354, 2951
Somov, B.V., & Titov, V. S. 1983, Sov. Astron. Lett., 9, 26
Sonnerup, B. U. O., & Priest, E. R. 1975, J. Plasma Phys., 14, 283
Spitzer, L. 1962, Physics of fully ionized gases (NewYork-London: Interscience Publishing)
Stanier, A., Browning, P., & Dalla, S. 2012, A&A, 542, A47
Tassi, E., Titov, V. S., & Hornig, G., 2005, Phys. Plasmas, 12, 112902
Titov, V. S., & Priest, E. R. 1997, J. Fluid Mech., 348, 327
Wyper, P. F., & Pontin, D. I. 2013, Phys. Plasmas, 20, 032117